Plasmonic extinction of gated graphene nanoribbon array analyzed by a scaled uniform Fermi level

Xiang-Tian Kong,[1] Xiaoxia Yang,[1] Zhenjun Li,[1] Qing Dai,[1,2] and Xiaohui Qiu[1,3]

[1]*National Center for Nanoscience and Technology, Beijing 100190, China*

[2]*e-mail: daiq@nanoctr.cn*

[3]*e-mail: xhqiu@nanoctr.cn*

Received October 31, 2013; revised January 22, 2014; accepted January 26, 2014;
posted January 27, 2014 (Doc. ID 200507); published March 4, 2014

A uniform Fermi level profile is typically assumed in the analysis of a gated graphene nanoribbon, whose Fermi level is actually nonuniform in the experimental measurements. Here, we show that the uniform Fermi level has to be downshifted when it is used to analyze a backgated graphene nanoribbon array (GNRA). The plasmonic extinction behaviors of the GNRAs are perfectly preserved by assuming properly scaled uniform Fermi levels. The scaling factor is independent of the average value of the actual Fermi level profile, but it is a function of the ratio of the nanoribbon width to the distance of the nanoribbons from the backgate. This study facilitates the data postprocessing in the experiments, and may be helpful for analyzing the electron behaviors in GNRAs.

OCIS codes: (240.6680) Surface plasmons; (160.4236) Nanomaterials; (260.2710) Inhomogeneous optical media.
http://dx.doi.org/10.1364/OL.39.001345

Theoretical and experimental works have shown that plasmons can be supported by graphene, a one-atom-thick graphite layer [1,2]. The graphene-based plasmons exhibit better field confinement in terahertz frequencies [3,4] compared with the plasmons supported by noble metals, and can be easily tuned by chemical [5,6] or electrostatic [7–11] doping. In particular, the confined plasmonic modes in graphene micro/nanoribbons have attracted much attention [4–8,12–16], partly because they can be excited directly by normally incident terahertz illuminations [5–8]. The plasmonic resonances were monitored by a characteristic extinction peak in the experimental studies [5–8], where the peak position (resonance frequency, ν_p) varied with the doping level (quantified through Fermi level, E_F) and the ribbon width, w.

In practice, the carrier density distribution in an electrostatically doped graphene ribbon is inhomogeneous, yielding a nonuniform Fermi level profile [17–19]. In contrast, chemical doping often yields uniform Fermi level profiles [6]. The plasmonic response of a graphene ribbon with a nonuniform Fermi level profile differs from that with a uniform Fermi level profile [19]. Nonetheless, the resonance frequency associated with the nonuniform Fermi level profile can be approximated by assuming a properly scaled uniform Fermi level [19]. Assuming uniform Fermi level simplifies the data processing in the experimental studies on gated graphene ribbons [6–8], and also facilitates the comparison between the experimental spectra of graphene structures with electrostatic doping and those with chemical doping.

In this Letter, we study the scaled uniform Fermi level (denoted by E_F^{eff}) in terms of the actual Fermi level profile of gated graphene ribbons and the geometry of the doping configuration. We focus on the first-order plasmonic resonance of graphene nanoribbon arrays (GNRAs) in the backgated configuration, owing to the great experimental interest [7,8]. The assumed uniform profile E_F^{eff} depends linearly on the average value of the actual Fermi level profile. The effect of assuming $E_F(x)$ equal to the uniform profile E_F^{eff} on the resonance frequency, as well as the extinction maximum of the backgated GNRAs, are discussed. Finally, we propose an expression for the relationship between the uniform Fermi level and the actual Fermi level profile induced by electrostatic doping.

The Fermi level profile of a graphene nanoribbon in the backgated configuration [inset of Fig. 1(a)] is obtained from the approach provided in [19]. Figure 1(a) shows the normalized Fermi level profiles, $E_F(x)/\langle E_F\rangle$, with

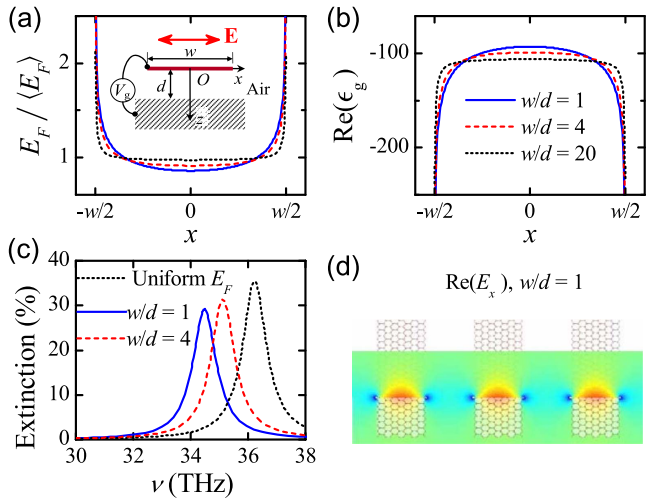

Fig. 1. (a) Fermi level profiles normalized to their average values of backgated graphene for $w/d = 1$ (solid), 4 (dashed), and 20 (dotted). The backgated configuration and light polarization direction are shown in the inset. (b) Equivalent relative permittivity (real part) of backgated graphene ($\langle E_F\rangle = 0.4$ eV). (c) Extinction spectra of a GNRA ($w = 100$ nm) with uniform Fermi level (dotted) and nonuniform Fermi level with $w/d = 1$ (solid) and $w/d = 4$ (dashed) under doping level of $\langle E_F\rangle = 0.4$ eV. (d) Snapshot of E_x near field of a backgated GNRA with $w = d = 100$ nm and $\langle E_F\rangle = 0.4$ eV at extinction maximum of 34.47 THz.

the ratio of the ribbon width to the distance between the nanoribbon and the backgate, w/d, equal to 1 (solid), 4 (dashed), and 20 (dotted). The profile tends to be flat as the ratio of w/d increases. The nonuniform profile approaches the uniform profile, i.e., $E_F(x) \to \langle E_F \rangle$, when w/d becomes extremely large. We characterize the Fermi level distribution by its average value and the ratio of w/d. The $E_F(x)$ profile of each nanoribbon in a GNRA is assumed to be identical to that of only one nanoribbon, ignoring the interaction of the adjacent nanoribbons.

The optical responses of GNRAs are simulated by using the finite element method. For simplicity, GNRAs are assumed to be freestanding under ambient conditions. The fraction of the array period occupied by the graphene nanoribbon is fixed at 1/2. The terahertz incident lights impinge perpendicularly on GNRAs. To implement the finite element calculations, the graphene is modeled as a material with a finite thickness and a phenomenological equivalent permittivity, which is thickness dependent. In our simulations, the graphene thickness (d_g) is set to be 1 nm, at which value the calculations reach proper convergence. The equivalent relative permittivity is derived from the two-dimensional conductivity of graphene and is given by $\epsilon_g = i\sigma/\epsilon_0 \omega d_g$ [9].

Here, ϵ_0 is the free space permittivity, $\omega = 2\pi\nu$ is the light angular frequency, and $\sigma = \sigma(\omega, E_F, \tau, T)$ is the complex conductivity of graphene calculated from the Kubo formula [20]. The relaxation time τ is obtained from $\tau = \mu E_F / e v_F^2$, where e is the electron charge, $\mu \approx 10,000\ \mathrm{cm}^2/(\mathrm{V}\cdot\mathrm{s})$ is the measured dc mobility, and $v_F \approx 1 \times 10^6$ m/s is the Fermi velocity [4]. The temperature T is assumed to be 300 K. Accordingly, the equivalent relative permittivity as a function of x can be obtained, as shown in Fig. 1(b), for $w/d = 1$ (solid), 4 (dashed), and 20 (dotted), under doping level of $\langle E_F \rangle = 0.4$ eV.

The extinction spectra of a GNRA with ribbon width $w = 100$ nm under doping level of $\langle E_F \rangle = 0.4$ eV for $d = 100$ nm, 25 nm, and 0 (uniform profile) are shown in Fig. 1(c). The resonant modes corresponding with the extinction maxima are the first-order plasmon modes, as confirmed by the E_x near field shown in Fig. 1(d). For a uniformly doped GNRA, the resonance frequency is determined by the doping level [7]. However, for a backgated GNRA, the resonance frequency moves to the higher frequencies as the ratio of w/d increases, with the average doping level being fixed [Fig. 1(c)]. Next, we first restrict ourselves to the case for $w/d = 1$ to obtain the relation between the assumed uniform Fermi level E_F^{eff} and the average Fermi level of the gated GNRAs. Then we discuss the dependence of E_F^{eff} on the ratio of w to d.

Figure 2(a) shows the dependence of the resonance frequency on the average Fermi level for the uniform (dashed) and nonuniform (solid) doping levels. The frequency of the plasmonic resonance increases with increasing doping level and decreases with increasing nanoribbon width. The resonance frequency of a GNRA with the actual nonuniform Fermi level profile is less than that with the uniform Fermi level profile for a fixed value of average Fermi level. Hence, the uniform Fermi level has to be downshifted in order to fit the resonance frequency with the actual Fermi level profile, when the

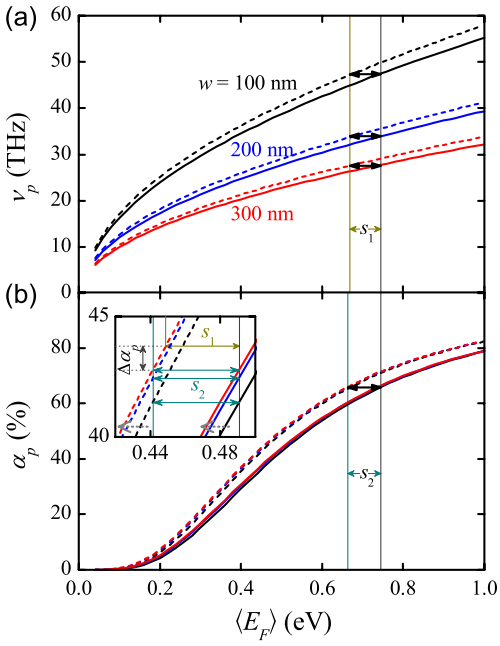

Fig. 2. Resonance frequency (a) ν_p and extinction maximum (b) α_p varying with the average Fermi level $\langle E_F \rangle$. Solid, nonuniform E_F profiles ($d = w$); dashed, uniform E_F profiles. In the inset of (b), w is equal to 100, 200, and 300 nm along the dashed arrows.

uniform Fermi level is assumed to describe the resonance frequency of the actually gated GNRA. We denote the difference between the average value of the actual Fermi level profile and the properly scaled uniform Fermi level by s_1, i.e., $s_1 = \langle E_F \rangle - E_F^{\mathrm{eff}}$. The curves of the resonance frequency in terms of the average Fermi level for the nonuniform and uniform profiles approach each other as the nanoribbon width increases. Nevertheless, the quantity s_1 is independent of the nanoribbon width at a fixed doping level, as shown in Fig. 2(a).

On the other hand, the extinction maximum (α_p) of a GNRA is mainly determined by the doping level. The extinction maximum increases with the increasing doping level for both the uniform and nonuniform Fermi level profiles [Fig. 2(b)]. The extinction maximum with the nonuniform Fermi level profiles is below that with the uniform Fermi level profiles. Consequently, a downshifted uniform Fermi level is required to achieve the same extinction maximum as the actual nonuniform Fermi level profile. We denote the difference between the average Fermi level of the actual profile and the required uniform Fermi level by s_2 [Fig. 2(b)]. Although the extinction maximum slightly increases as the ribbon width w increases at a fixed average Fermi level, the quantity s_2 is found to be independent of the nanoribbon width, as shown in the inset of Fig. 2(b). We note that the independence of s_1 and s_2 of the nanoribbon width with fixing the ratio of w to d is attributed to the similarity of the Fermi level profiles associated with different nanoribbon widths.

Both the quantities of s_1 and s_2 are proportional to the average Fermi level of the actually gated GNRAs for a fixed ratio of w to d [Fig. 3(a)]. They can be expressed by

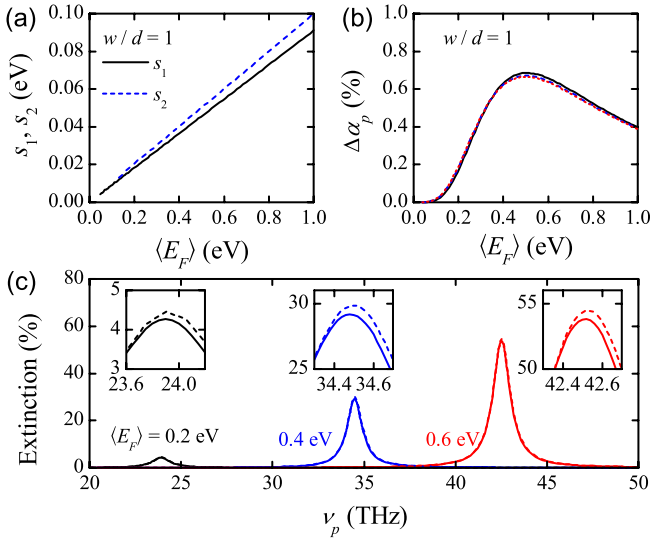

Fig. 3. (a) The quantities of s_1 and s_2 varying with the average Fermi level for $w/d = 1$. (b) The same for $\Delta\alpha_p$. The solid, dashed, and dotted lines correspond with $w = 100$, 200, and 300 nm, respectively. (c) Extinction spectra of GNRA with $w = 100$ nm and $\langle E_F\rangle = 0.2$, 0.4, and 0.6 eV for the actual Fermi level profiles (solid) and the uniform Fermi levels given by $E_F^{\text{eff}} = 0.91\langle E_F\rangle$ (dashed). Insets show the zoomed regions around the extinction peaks.

$$s_1 = 0.09\langle E_F\rangle, \qquad s_2 = 0.1\langle E_F\rangle, \qquad (\text{for } w/d = 1) \quad (1)$$

respectively, for the configuration with $w/d = 1$, according to linear curve fitting processes. Hence, the required uniform Fermi level given by $E_F^{\text{eff}} = \langle E_F\rangle - s_1$ is also proportional to the average Fermi level. We note that both the proportionality relations of s_1 and s_2 with respect to the average Fermi level are independent of the nanoribbon width. The quantity s_1 is always less than the quantity s_2 at a fixed doping level. Accordingly, the extinction maximum of a GNRA with the scaled uniform Fermi level E_F^{eff} deviates from that of the actually gated GNRA.

We denote the extinction maximum of a GNRA with the actual Fermi level profile subtracted from that with the uniform Fermi level E_F^{eff} by $\Delta\alpha_p$ [inset of Fig. 2(b)]. The quantity $\Delta\alpha_p$ can be written as $\Delta\alpha_p = (s_2 - s_1)\,\partial\alpha_p/\partial E_F$, where the derivation is in connection with the uniform Fermi level profiles. Figure 3(b) shows the dependence of $\Delta\alpha_p$ on the average of the actual Fermi level profile. The quantity $\Delta\alpha_p$ is almost independent of the nanoribbon width, and increases from 0 to a maximum and decreases as the average Fermi level increases from 0 to 1 eV. The maximum of $\Delta\alpha_p$ appears at the doping level of $\langle E_F\rangle = 0.50$ eV and is approximately equal to 0.7%.

Figure 3(c) shows the extinction spectra of the GNRA with $w = 100$ nm for the actual Fermi level profiles (solid) and the scaled uniform Fermi level profiles E_F^{eff} (dashed) at doping levels $\langle E_F\rangle = 0.2$, 0.4, and 0.6 eV. Only very small distinctions can be observed between the actual extinction spectra and corresponding spectra with the scaled uniform Fermi level E_F^{eff} [see the zoomed regions around the extinction peaks in the insets of Fig. 3(c)]. Moreover, the line shapes of the extinction spectra are also well preserved. Thus, the deviation resulting from the assumption of the uniform Fermi level of E_F^{eff} can be ignored in most of the practical cases. And all the features of the plasmonic extinction behaviors of GNRAs can be described by using the scaled uniform Fermi level.

Since the resonance frequency increases when the Fermi level profile in a gated GNRA becomes flatter [Fig. 1(b)], the scaled uniform Fermi level E_F^{eff} also depends on the geometry of the backgated configuration. The quantity s_1 can be easily obtained with the knowledge that it is linearly dependent on the average Fermi level for a given ratio of w to d. Figure 4(a) shows the slope of s_1 with respect to the average Fermi level, $\partial s_1/\partial\langle E_F\rangle$, as a function of the ratio of w to d. The slope of s_1 decreases with increasing w/d. For small values of w/d, the Fermi level profile of a gated GNRA approaches the narrow ribbon limit [19], and the slope of s_1 approaches a maximum. For large values of w/d, the Fermi level profile tends to be flat, resulting in the slope of s_1 being nearly zero.

The slope of s_1 can be calculated from

$$\frac{\partial s_1}{\partial\langle E_F\rangle} = \begin{cases} [(w/d)^3 - 6.2(w/d)^2 + 96]/1000, & w/d \le 3 \\ 0.12(w/d)^{-0.41}\exp(-0.042w/d), & w/d > 3 \end{cases}, \quad (2)$$

according to least square fitting of the computed data [see Fig. 4(a) and the inset]. Then the scaling factor, which is defined by $f = \partial E_F^{\text{eff}}/\partial\langle E_F\rangle = 1 - \partial s_1/\partial\langle E_F\rangle$, can be written as

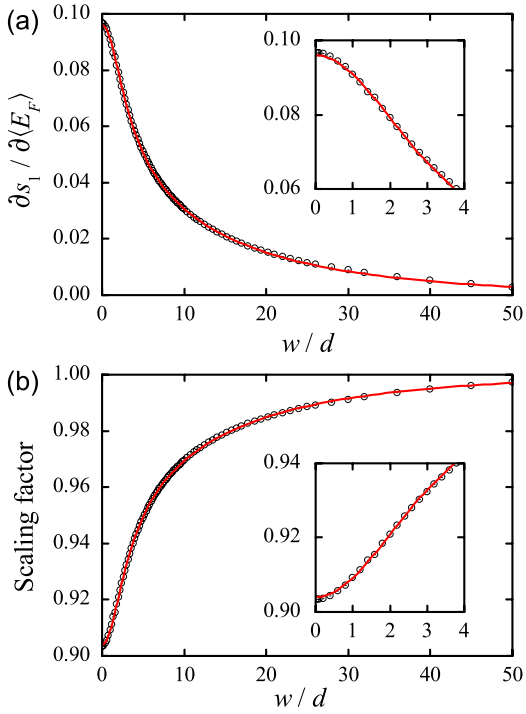

Fig. 4. (a) Dependence of the derivative of s_1 with respect to the average Fermi level on w/d. (b) The same for the scaling factor, f. Circles show the computed data. Lines in (a) and (b) are fitted curves given by Eqs. (2) and (3), respectively. Insets show the zoomed regions for small w/d.

$$f = \begin{cases} [-(w/d)^3 + 6.2(w/d)^2 + 904]/1000, & w/d \le 3 \\ 1\text{–}0.12(w/d)^{-0.41}\ \exp(-0.042w/d), & w/d > 3 \end{cases}, \tag{3}$$

and the scaled uniform Fermi level can be written as

$$E_F^{\text{eff}} = f\langle E_F \rangle. \tag{4}$$

As shown in Fig. 4, large values of w/d need small corrections of the Fermi level. When the ratio of w to d exceeds 10, less than 3% of the Fermi level needs to be shifted and the scaling factor is more than 0.97.

In conclusion, the extinction behaviors of the plasmonic resonances in a gated GNRA can be perfectly analyzed by a properly downshifted uniform Fermi level. The scaled uniform Fermi level is proportional to the average value of the actual nonuniform Fermi level profile for a fixed ratio of the nanoribbon width to the distance of the nanoribbon from the backgate, w/d. We have provided a quantitative study on the scaling factor in terms of w/d. The expression of the scaled uniform Fermi level is useful for data processing in the experimental studies on plasmonic responses of GNRAs, and enables accurate comparison between the plasmonic responses of GNRAs with electrostatic doping and those with chemical doping. Our proposed model may be extended to investigate electronic properties of graphene nanoribbons, especially nanoribbons with very narrow widths [21].

This work is supported by the National Natural Science Foundation of China (51372045).

References

1. F. J. G. de Abajo, Science **339**, 917 (2013).
2. F. H. L. Koppens, D. E. Chang, and F. J. G. de Abajo, Nano Lett. **11**, 3370 (2011).
3. M. Jablan, H. Buljan, and M. Soljacic, Phys. Rev. B **80**, 245435 (2009).
4. J. Christensen, A. Manjavacas, S. Thongrattanasiri, F. H. L. Koppens, and F. J. G. de Abajo, ACS Nano **6**, 431 (2012).
5. J. H. Strait, P. Nene, W.-M. Chan, C. Manolatou, S. Tiwari, F. Rana, J. W. Kevek, and P. L. McEuen, Phys. Rev. B **87**, 241410 (2013).
6. H. Yan, T. Low, W. Zhu, Y. Wu, M. Freitag, X. Li, F. Guinea, P. Avouris, and F. Xia, Nat. Photonics **7**, 394 (2013).
7. L. Ju, B. Geng, J. Horng, C. Girit, M. Martin, Z. Hao, H. A. Bechtel, X. Liang, A. Zettl, Y. R. Shen, and F. Wang, Nat. Nanotechnol. **6**, 630 (2011).
8. V. W. Brar, M. S. Jang, M. Sherrott, J. J. Lopez, and H. A. Atwater, Nano Lett. **13**, 2541 (2013).
9. A. Vakil and N. Engheta, Science **332**, 1291 (2011).
10. P.-Y. Chen and A. Alu, ACS Nano **5**, 5855 (2011).
11. W. Gao, G. Shi, Z. Jin, J. Shu, Q. Zhang, R. Vajtai, P. M. Ajayan, J. Kono, and Q. Xu, Nano Lett. **13**, 3698 (2013).
12. V. V. Popov, T. Y. Bagaeva, T. Otsuji, and V. Ryzhii, Phys. Rev. B **81**, 073404 (2010).
13. S. He, X. Zhang, and Y. He, Opt. Express **21**, 30664 (2013).
14. X. Shi, D. Han, Y. Dai, Z. Yu, Y. Sun, H. Chen, X. Liu, and J. Zi, Opt. Express **21**, 28438 (2013).
15. J. T. Kim, Y.-J. Yu, H. Choi, and C.-G. Choi, Opt. Express **22**, 803 (2014).
16. J. Tao, X. Yu, B. Hu, A. Dubrovkin, and Q. J. Wang, Opt. Lett. **39**, 271 (2014).
17. P. G. Silvestrov and K. B. Efetov, Phys. Rev. B **77**, 155436 (2008).
18. F. T. Vasko and I. V. Zozoulenko, Appl. Phys. Lett. **97**, 092115 (2010).
19. S. Thongrattanasiri, I. Silveiro, and F. J. G. de Abajo, Appl. Phys. Lett. **100**, 201105 (2012).
20. V. P. Gusynin, S. G. Sharapov, and J. P. Carbotte, J. Phys. Condens. Matter **19**, 026222 (2007).
21. X. Li, X. Wang, L. Zhang, S. Lee, and H. Dai, Science **319**, 1229 (2008).